Inorganic Chemistry

Article

pubs.acs.org/IC

Electronic and Photophysical Properties of Platinum(II) Biphenyl Complexes Containing 2,2′-Bipyridine and 1,10-Phenanthroline Ligands

D. Paul Rillema,*[,†] Arvin J. Cruz,[‡] Curtis Moore,[†] Khamis Siam,[‡] A. Jehan,[†] Derek Base,[‡] T. Nguyen,[†] and Wei Huang[†]

[†]Department of Chemistry, Wichita State University, Wichita, Kansas 67260, United States

[‡]Department of Chemistry, Pittsburgh State University, Pittsburgh Kansas 66762, United States

Supporting Information

ABSTRACT: Pt(bph)(bpy) and Pt(bph)(phen), where bph is the 2,2′-biphenyl dianion, bpy is 2,2′-bipyridine, and phen is 1,10-phenanthroline, crystallize in the space groups $I4_1/a$ and $P2_1/c$, respectively, in two different configurations as X-shaped and bowed (B). The distance between Pt centers is 3.5 Å indicative of $\pi-\pi$ stacking. The complexes are optically active, absorb light at 440 nm, and emit in the solid state at room temperature and in the solid glass phase at 77 K. The emission maxima for both in the glass occur near 581 nm but are red-shifted to ∼700 nm in the solid state. Both complexes exhibit solvatochromism in nitrile-based solvents with the Pt(bph)(phen) complex showing greater excited state dipole character compared to the Pt(bph)(bpy) derivative. Frontier orbitals for the HOMO determined by DFT calculations contain electronic contributions from the biphenyl ligand and the platinum center. The LUMO orbitals primarily reside on the diimine ligands. TDDFT calculations indicate the low-energy transitions occur from the metal/bph combination to the diimine ligand.

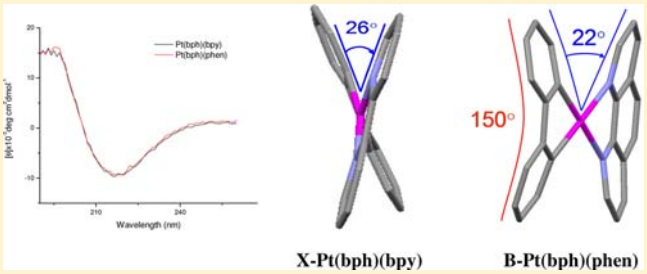

INTRODUCTION

Square planar platinum(II) complexes containing bidentate biphenyl chelating ligands are attractive emitters[1−3] with promising applications in optoelectronic devices,[4] chemosensory materials, and catalysis.[5] The complexes display rich emission properties both in solution[1−3,6] and in the solid state.[7] In dilute solution, emission was assigned either to a ^{3}LC or a ^{3}MLCT state,[2,3,6] but in more concentrated solution aggregation gave rise to different emission maxima.[7] The platinum(II) biphenyl dicarbonyl complex was also found to undergo $\pi-\pi$ stacking in the solid state resulting in electronic interactions associated with Pt···Pt orbital overlap.[8] The Pt(bph)(bpy) complex[1] was reported in the past while, to our knowledge, the Pt(bph)(phen) derivative was not. The absorption spectrum showed a broad peak located at 429 nm (ε = 5700 M^{-1} cm^{-1}) plus additional bands related to intraligand transitions at higher energy. An emission maximum was observed at 581 nm with an emission lifetime of 1.1 μs at 77 K in a butyronitrile glass upon excitation at 355 nm. The low-energy absorption band was also reported to be solvent dependent.[9]

This paper describes our goal of obtaining a better understanding of the electronic structures and photophysical properties of Pt(bph)(bpy) and Pt(bph)(phen), where bph is the 2,2′-biphenyl dianion, bpy is 2,2′-bipyridine, and phen is 1,10-phenanthroline. A modified synthetic procedure for the synthesis of Pt(bph)(bpy) and Pt(bph)(phen) is given, and their single X-ray structures and spectroscopic and luminescence properties are described. The strong field dianionic bph ligand is expected to drive up the energy of the d−d state on the metal center enhancing emission and to have higher π^* energy levels than the diimine ligands. Consequently, the LUMO is expected to reside on the diimine ligands, which can be verified by DFT and TDDFT calculations.

EXPERIMENTAL SECTION

General Procedures and Chemicals. All syntheses were performed under a dry and oxygen-free nitrogen atmosphere, using standard Schlenk-ware techniques. Anhydrous diethyl ether (99.7%) and anhydrous tetrahydrofuran, THF (99.9%), were used as received from Aldrich. The other solvents, methylene chloride, hexanes, butyronitrile, propionitrile, valeronitrile, and acetonitrile, were used without further purification. Potassium tetrachloroplatinate(II) was purchased from Alfa Aesar. The ligand 2,2′-dipyridyl was purchased from ACROS and 1,10-phenanthroline monohydrate was purchased from GFS. Diethyl sulfide and *n*-butyl lithium were purchased from Aldrich. 2,2′-Dibromobiphenyl,[10] 2,2′-dilithiobiphenyl,[11] and $[PtCl_2((C_2H_5)_2S)_2]$[12] were prepared according to published procedures. $[Pt(bph)(SEt_2)]_2$ was prepared by a modification of the one published procedure.[2,9]

Preparation of $[Pt(bph)(SEt)_2]_2$. As shown in Figure 1a, the compound was prepared via two parallel steps. First, the biphenyl dianion was prepared in Schlenk-ware consisting of a round-bottomed

Received: June 28, 2012
Published: December 27, 2012

   dx.doi.org/10.1021/ic301393e | *Inorg. Chem.* 2013, 52, 596−607

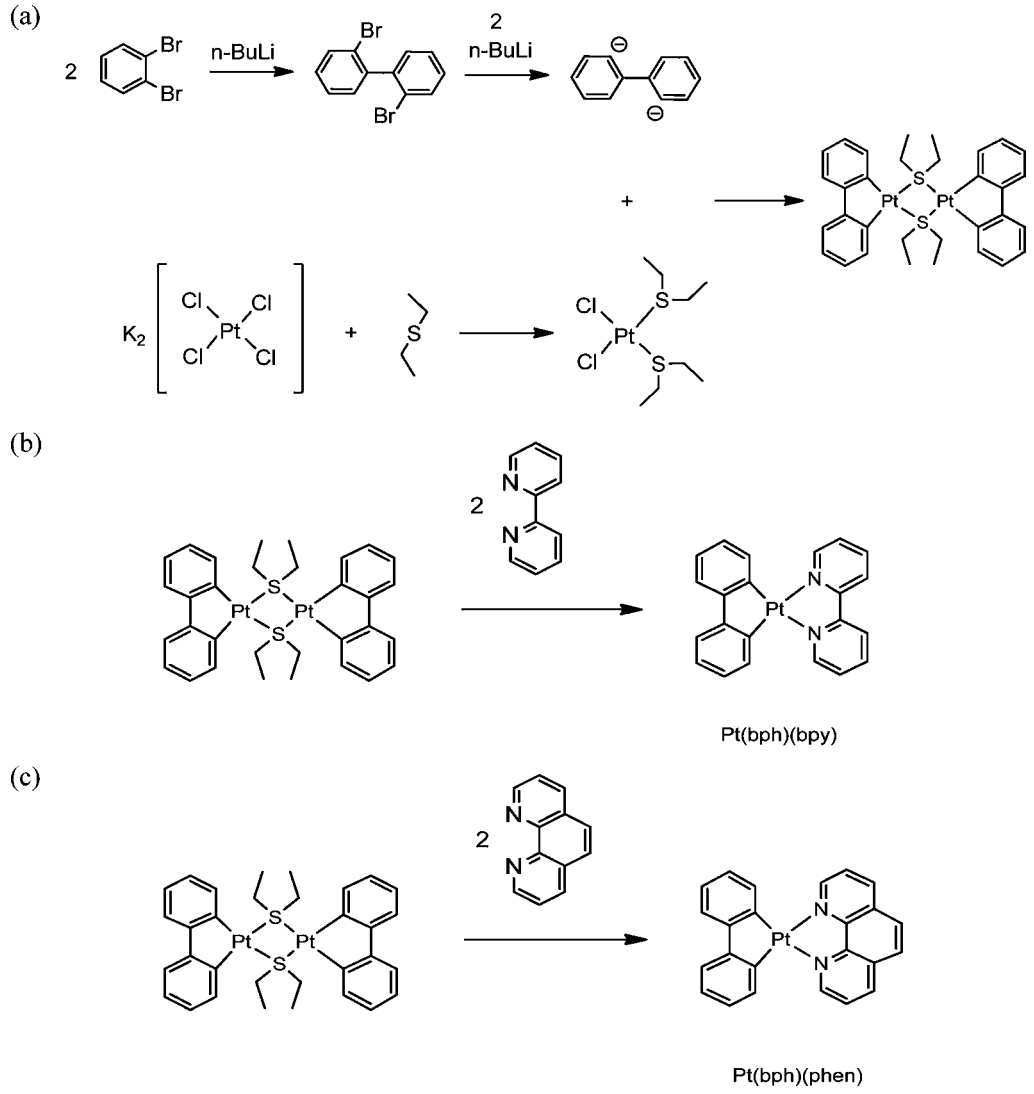

Figure 1. Preparation of (a) $[Pt(bph)(SEt_2)]_2$, (b) Pt(bph)(bpy), and (c) Pt(bph)(phen).

flask connected by a T-tube to a dropping funnel. A serum cap was wired into place on the top of the T-tube containing 840 mg of 2,2′-dibromobiphenyl (2.6 mmol) and a magnetic stirring bar. Then the apparatus was evacuated three times and refilled with dry N_2 each time. Then 40 mL of dry ether was cannulated into the flask. The temperature of the contents in the flask was lowered to −70 °C with a dry ice/isopropanol bath. Then 2.1 mL of *n*-butyl lithium solution (2.5 M; 5.2 mmol) was added dropwise, using a gastight syringe over a 2 h period. The solution containing the biphenyl dianion was then allowed to warm to 0 °C for 2 h and then was transferred to a dropping funnel that was connected to the T-tube.

For the second step, a second round-bottomed flask containing 1.2 g of $Pt((C_2H_5)_2S)_2Cl_2$ (2.6 mmol) and a magnetic stirring bar was fitted with a serum cap on top. The flask was evacuated three times and refilled with dry N_2 each time. Then about 40 mL of dry ether was cannulated into the flask. Then the dropping funnel from step one and the flask were rapidly connected, the system was flushed with N_2, partially evacuated (to not evaporate too much ether) two to three times, and refilled with dry N_2 each time. The contents of the flask were cooled in an ethylene glycol−dry ice bath (−30 to −40 °C) and the contents of the dropping funnel were added over a 2 h period. The orange-brown solution was stirred overnight and allowed to warm to room temperature. The next day the solution gave a darker coloration. The suspension was vacuum filtered and the dark yellow solid crude product was collected (∼1.20 g) while the filtrate was discarded. The crude sample was then dissolved in a minimum amount of methylene chloride (DCM). Ether was then added dropwise into the DCM solution until a yellow precipitate started forming. The volume was reduced under the hood for 30 min. The mixture was then filtered and 0.57 g of fine yellow product was collected. Yield = 49%. One spot was found by TLC for the compound; ^{1}H NMR ($CDCl_3$): δ 7.32 (dd, 2H, J = 7.5, 1.3 Hz), 7.03 (ddd, 2 H, J = 7.3, 1.09 Hz), 6.98 (dd, 2H, J = 7.4, 1.1 Hz), 6.88 (ddd, 2H, J = 7.4, 1.4 Hz), 3.82 (q, 4H, J = 7.4 Hz), 1.75 (t, 6H, J = 7.4 Hz).

Preparation of Complexes. *Pt(bph)(bpy).* A solution was prepared by dissolving 0.12 g (0.77 mmol) of 2,2′-dipyridyl and 0.30 g (0.34 mmol) of $[Pt(bph)(C_2H_5)_2S]_2$ in 20 mL of methylene chloride in a 50-mL round-bottomed flask (Figure 1b). The mixture immediately changed from a yellow-orange to a dark red color. A stir bar was added and the flask was attached to a condenser, placed on top of a heating mantle, and set to reflux for 30 min. The solution had then become an even darker blood-red color. The solution was then suction filtered, which yielded minute amounts of red crystals on the filter paper. The filtrate portion was covered with parafilm and placed in the freezer overnight. After 8 h, fine red crystals of the compound had formed. A 1 × 1 × 1 mm^3 single crystal was handpicked and analyzed by X-ray crystallography. The rest of the crystals (0.21 g) were collected via vacuum filtration. Yield = 58%. Anal. Calcd for $C_{22}H_{16}N_2Pt$: C, 52.48; H, 3.20; N, 5.56. Found: C, 52.11; H, 3.09; N, 5.44. IR (KBr pellet): 3044, 1599, 1445, 1424, 1065, 738, 699 cm^{-1}. ^{1}H NMR ($CDCl_3$): δ 9.67 (d, 2H, J = 5.6 Hz), 8.18 (td, 2H, J = 5.6, 1.6 Hz), 8.13 (dd, 2H, J = 5.6, 1.6 Hz), 7.65 (td, 2H, J = 5.6, 1.6 Hz),

dx.doi.org/10.1021/ic301393e | *Inorg. Chem.* 2013, 52, 596−607

7.47 (dd, 2H, J = 6.8, 2.0 Hz), 7.39 (dd, 2H, J = 6.8, 2.0 Hz), 7.01 (td, 2H, J = 6.8, 2.0 Hz), 6.97 (td, 2H, J = 6.8, 2.0 Hz).

Pt(bph)(phen). A solution was prepared by dissolving 0.090 g (0.45 mmol) of 1,10-phenanthroline monohydrate and 0.20 g (0.22 mmol) of $[Pt(bph)(C_2H_5)_2S]_2$ in 20 mL of methylene chloride (Figure 1c). The mixture immediately turned from yellow to a red-orange color. A stir bar was added and the flask was attached to a condenser, placed on top of a heating mantle, and set to reflux for approximately 1 h to make certain that yellow starting materials were completely reacted. After reflux, the mixture was allowed to cool to room temperature and filtered. The filtrate was collected, transferred into a clean container, and left in the freezer overnight. After approximately 8 h, dark red crystals of Pt(bph)(phen) formed. In a similar fashion, a single crystal was handpicked and examined by X-ray crystallography. The remaining crystals were collected via vacuum filtration. Yield = 37%. Anal. Calcd for $C_{24}H_{16}N_2Pt$: C, 54.65; H, 3.06; N, 5.31. Found: C, 54.45; H, 3.07; N, 5.27. IR (KBr pellet): 3041, 1653, 1581, 1426, 1419, 1021, 840, 743, 717 cm^{-1}. ^1H NMR (CD_2Cl_2): δ 9.93 (dd, 2H, J = 5.2, 1.2 Hz), 8.69 (dd, 2H, J = 8.0, 1.2 Hz), 8.02 (s, 2H), 8.00 (dd, 2H, J = 8.0, 5.2 Hz), 7.55 (dd, 2H, J = 6.8, 2.0 Hz), 7.34 (dd, 2H, J = 6.8, 2.0 Hz), 6.97 (m, 4H, J = 6.8, 2.0 Hz).

Instrumentation and Physical Measurements. UV−vis spectra were obtained with an OLIS modernized Cary 14 spectrophotometer. The IR spectra were acquired with a Nicolet Avatar 360 FT-IR spectrophotometer. Proton NMR spectra were obtained with a Varian Inova 400 FT-NMR spectrometer. Elemental (C, H, and N) analysis was performed by MHW Laboratories. CD spectra were obtained with a Jasco J-810 CD Spectrometer interfaced with a Jasco Spectral Analysis software program compatible with Windows Operating System. CD measurements were made in butyronitrile solutions with absorbances near 0.8 (5 cm cells). An EG&G PAR Model 263A potentiostat/galvanostat was used to obtain the cyclic voltammograms. The measurements were carried out in a typical H-cell with use of a platinum disk working electrode, a platinum wire counter electrode, and a Ag/AgCl reference electrode in acetonitrile. The supporting electrolyte used was 0.1 M tetrabutylammonium hexafluorophosphate ($TBAPF_6$). Ferrocene was added as the reference.

Corrected emission spectra and emission lifetimes were collected with a HoribaJobinYvon Nanolog spectrometer. Emission spectra and emission lifetimes were obtained from 0.1 absorbing solutions in butyronitrile at 77 K. The excitation wavelength was 440 nm for obtaining emission spectra; a NanoLED-460 was the excitation source for emission lifetime determinations. The emission curve fittings were performed with the Origin Pro 8 program via nonlinear curve-fitting modes.

Calculations. Calculations were effected by using Gaussian '03 (Rev. B. 03) for UNIX.[13] The molecules were optimized by using Becke's three-parameter hybrid functional B3LYP[14] with the local term[15] of Lee, Young, Parr and the nonlocal term[16] of Vosko, Wilk, and Nassiar. The basis set SDD[17] was chosen for all atoms and geometry optimizations were all ran in the gas phase. TDDFT[18] calculations were employed to produce a number of singlet excited states[19] in the gas phase based on the optimized geometry. Electronic absorption spectra of the complexes were generated by using the Gaussum 2.1.[20,21]

RESULTS

X-ray Crystallographic Data Collection. The crystals were obtained by slow evaporation of the reaction mixture in saturated methylene chloride. All crystals were affixed to a nylon cryoloop with oil (Paratone-n, Exxon) and mounted in the cold stream of a Bruker Kappa-Apex-II area-detector diffractometer.[22] The temperature was maintained at 100 K for Pt(bph)((bpy)·CH_2Cl_2 and at 150 K for Pt(bph)(phen) by using a Cryostream 700EX Cooler (Oxford Cryosystems). The unit cells were determined from the setting angles of 220 reflections for Pt(bph)(phen) and 276 reflections for Pt(bph)(bpy) collected in 36 frames of data. Data were measured with a redundancy of 15.6 for Pt(bph)(phen) and 9.16 for Pt(bph)(bpy) with a CCD detector at a distance of 40 mm for Pt(bph)(phen) and 50 mm for Pt(bph)(bpy) from the crystal with a combination of phi and omega scans. A scan width of 0.3° for Pt(bph)(phen) and 0.5° for Pt(bph)(bpy) and time of 10 s were employed along with graphite monochromatic Molybdenum Kα radiation (λ = 0.71073 Å) that was collimated to a 0.3 mm diameter for Pt(bph)(phen) and a 0.6 mm diameter for Pt(bph)(bpy). Data collection, reduction, structure solution, and refinement were performed with the Bruker Apex2 suite (v2.0−2).[22] All available reflections to $2\theta_{max}$ = 52° were harvested (47701 for Pt(bph)(phen) and 127144 for Pt(bph)(bpy), 3311 unique for Pt(bph)(phen) and 7121 unique for Pt(bph)(bpy)) and corrected for Lorentz and polarization factors with Bruker SAINT (v6.45).[22a,b] Reflections were then corrected for absorption (numerical correction, μ = 7.414 mm^{-1}), interframe scaling, and other systematic errors with SADABS 2004/1 (combined transmission and other correction factors min/max = 0.2692/0.4457 for Pt(bph)(phen) and 0.3009/0.7994 for Pt(bph)(bpy)). The structures were solved (direct methods) and refined (full-matrix least-squares against F^2) with the Bruker SHELXTL package (v6.14−1).[22] All non-hydrogen atoms were refined with use of anisotropic thermal parameters. All hydrogen atoms were included at idealized positions; hydrogen atoms were not refined. Pertinent crystal, data collection, and refinement parameters are given in Table 1. (See Tables S1−S10 in the Supporting Information for additional crystallographic data.)

X-ray Crystal Structure Determination and DFT Optimization. Figure 2 shows the ORTEP[22c] structures (single molecule and stacked) of Pt(bph)(bpy) and Pt(bph)-(phen) determined by X-ray crystallography. Selected bond distances and angles are given in Table 2 as well as values from calculations. Pt−C and Pt−N bond lengths are between 1.99 and 2.01 Å and 2.10 and 2.12 Å, respectively, which are normal compared to other similar complexes.[8,23−26]

The compound Pt(bph)(phen) sits on a general position in the monoclinic space group $P2_1/c$ and Pt(bph)(bpy) in the tetragonal space group $I4_1/a$. Both complexes were stacked in pairs in the solid state (Figure 2). The distances between platinum−platinum centers are 3.507 Å in Pt(bph)(bpy) and 3.387 Å in Pt(bph)(phen), which corresponds to a Pt···Pt distance associated with $\pi-\pi$ stacking in other platinum(II) square-planar complexes.[8,24,27−34]

To gain further insight, experimental data were correlated with theoretical results. Geometry optimization was performed by using density functional theory (DFT) and compared with actual crystal structures. The calculated parameters agree with the values determined from the X-ray structures.

Electronic Absorption Spectra. Figure 3 shows the absorption spectra of Pt(bph)(bpy) in butyronitrile solution and in the solid state (KBr pellet). Absorption and emission data for both complexes are listed in Table 3. Extinction coefficients of major transitions were determined from Beer's law studies, using five dilution points, and are listed in Table 3. There are three bands located between 400 and 500 nm, 290−350 nm, and <290 nm regions. The band centered near 440 nm is broad; the intermediate absorption occurs on a shoulder of the more intense absorption at highest energy. The absorption spectrum of solid Pt(bph)(bpy) in KBr pellet is shown in Figure 3b and is similar to the visible spectrum of the one in solution. Ligand reduction potentials are also presented in Table 3.

dx.doi.org/10.1021/ic301393e | Inorg. Chem. 2013, 52, 596−607

Table 1. Crystal Data and Structure Refinement for Pt(bph)(phen) and Pt(bph)(bpy)

complex	Pt(bph)(phen)	Pt(bph)(bpy)·CH_2Cl_2
empirical formula	$C_{24}H_{16}N_2Pt_1$	$C_{23}H_{18}Cl_2N_2Pt$
formula wt	527.48	588.38
temperature	150 K	100 K
wavelength	0.71073 Å	0.71073 Å
crystal system	monoclinic	tetragonal
space group	$P2_1/c$	$I4_1/a$
unit cell dimensions	a = 10.1828(6) Å	a = 38.6769(7) Å
	b = 13.9182(8) Å	b = 38.6769(7) Å
	c = 12.8693(7) Å	c = 9.7217(4) Å
	α = 90°	α = 90°
	β = 112.509(3)°	β = 90°
	γ = 90°	γ = 90°
volume	1684.97(17) Å^3	14542.7(7) Å^3
Z	4	32
calcd density	2.079 g/cm^3	2.150 g/cm^3
absorption coeff	8.338 mm^{-1}	8.025 mm^{-1}
F(000)	1008	9024
crystal size	0.24 × 0.18 × 0.16 mm^3	0.19 × 0.06 × 0.04 mm^3
crystal habit	block	prism
crystal color	lustrous dark purple	lustrous dark red
θ range for data collection	2.25° to 26.00°	3.16° to 26.00°
limiting indices	$-12 \le h \le 12$	$-47 \le h \le 47$
reflcns collected/ unique	47701/3311 [R(int) = 0.0494]	127144/7121 [R(int) = 0.1030]
completeness to θ = 26.00	100%	99.8%
refinement method	full-matrix least-squares on F^2	full-matrix least-squares on F^2
data/restraints/ parameters	3311/0/244	7121/12/451
refinement threshold	$I > 2\sigma(I)$	$I > 2\sigma(I)$
data > threshold	2986	5039
goodness-of-fit on F^2	1.059	1.057
final R indices [$I > 2\sigma(I)$]	R1 = 0.0156, wR2 = 0.0335	R1 = 0.0552, wR2 = 0.1204
R indices (all data)	R1 = 0.0193, wR2 = 0.0347	R1 = 0.0852, wR2 = 0.1301
largest diff peak and hole	0.727 and −0.603 e$^-$ Å^{-3}	2.325 and −1.075 e$^-$ Å^{-3}

Solvatochromism. Results from solvent-dependence studies are presented in Table 4 where the absorption maxima are expressed in wavenumbers (cm^{-1}). Solvents used in the experiment are all nitrile based with varying alkyl chain length. Solvent dielectric constants and refractive indices are listed in the second and third columns. Absorption maxima of the MLLCT (Metal−Ligand-to-Ligand Charge Transfer) band in both complexes are written in latter columns. Figure 4 shows solvatochromic behavior of the MLLCT absorption energy for the Pt(bph)(bpy) complex.

Circular Dichroism. CD spectra of both complexes in butyronitrile as shown in Figure 5 are similar. Two spectral features were observed, one in the visible region with peaks near 425 nm and the other in the ultraviolet region of the spectrum with peaks at ∼215 nm. This feature of the complexes is most likely structurally related.[35,36]

Emission Data. Figure 6 shows the emission spectrum of Pt(bph)(bpy) in a butyronitrile glass at 77 K and the room temperature emission spectrum of the complexes in the solid state, which is red-shifted approximately 150 nm compared to the glassy matrix. Pt(bph)(bpy) has an emission wavelength, λ_{em}, centered at 578 nm. Pt(bph)(phen) also gave rise to low-temperature emission in butyronitrile glass at 77 K with its maximum located at ∼580 nm. Vibronic structure was observed for both complexes but is more defined for the phenanthroline derivative. The emission lifetimes at 77 K were 0.95 ns for Pt(bph)(bpy) and 3.61 ns for Pt(bph)(phen), respectively.

DISCUSSION

Synthesis. Modification of the procedure for the synthesis of $[Pt(bph)(CH_3CH_2)_2S]_2$ gave a remarkable improvement in product yield from 17% to 49% compared to earlier preparation procedures[2,3] reported. The temperature control and slow warming process seems to be critical in this reaction. On preparation of Pt(bph)(phen) and Pt(bph)(bpy), instead of adding $[Pt(bph)(CH_3CH_2)_2S]_2$ into melted bpy or phen as reported by Cornioley-Deuschel and von Zelwesky,[12] the reaction was carried out in solution with methylene chloride as the solvent.

Structures. The coordination sphere of the platinum center in the solid state is not perfectly square planar for both Pt(bph)(bpy) and Pt(bph)(phen). An edge view of the Pt(bph)(bpy) complex shown in Figure 7 reveals that the bph and bpy ligands cross one another giving rise to an X configuration. Diffraction data indicate a cross-angle of 26° with respect to the platinum metal center.

The ligands of Pt(bph)(phen) complex behave differently. One finds that the rings of the bph ligand and those of the phen ligand bow (B-configuration) with an angle of 22° with respect to the platinum center resulting in a pseudobutterfly arrangement. A 20° C−C−N−N torsion angle is found for the X shape configuration, but only a 0.3° C−C−N−N torsion angle for the B shape configuration.

The bow-shaped (B-configuration) behavior was exhibited by $Pt(bpy)_2(TCNQ)_3$[26] and $Pt(bpy)_2(TCNQ)_2$.[25] The X-shaped structure of Pt(bph)(bpy) is clearly shown in Figure 7. In a similar fashion, the X-shaped structure has also been found in other platinum and palladium complexes such as $Pt(phen)Cl_2$[27] and $Pd(phen)_2(ClO_4)_2$.[37] The angle of distortion from the axis of planarity in the X-shaped Pt(bph)(bpy) is 26° and compared to 24° for $Pt(bpy)_2(NO_3)_2·H_2O$.[38] As noted in Figure 5, both the B-form and X-form display chirality. This behavior is due to its lack of symmetry and can be attributed to complexes exhibiting the C_1 point group.[39]

Geometry optimizations have been conducted with DFT. In the optimization process, different basis sets have been tried including MP2/SDD,[17,40−42] MP2/LanL2DZ,[39,42−44] and DFT/SDD[17−19,44] in order to check which configuration gave the minimum energy. According to the results, the X-form is always the preferred configuration compared to the B form in both Pt(bph)(bpy) and Pt(bph)(phen). The minimum energies for the Pt(bph)(phen) X form were 2.79 × 10^{-3} eV (MP2/SDD), 2.42 × 10^{-3} eV (MP2/LanL2DZ), and 2.88 × 10^{-3} eV (DFT/SDD), respectively; minimum energies for the B form were 2.88 × 10^{-3} eV (MP2/SDD), 2.84 × 10^{-3} eV (MP2/LanL2DZ), and 3.59 × 10^{-3} eV (DFT/SDD), respectively. Crystal packing may account for the observation of the B form.

Population Analysis. Theoretical calculations are useful to gain intuition about the electron density localization in both occupied and unoccupied molecular orbitals. This helps one to trace how electrons are tunneled within the different functional groups of the complexes. Also, it is helpful in identifying the key

dx.doi.org/10.1021/ic301393e | Inorg. Chem. 2013, 52, 596−607

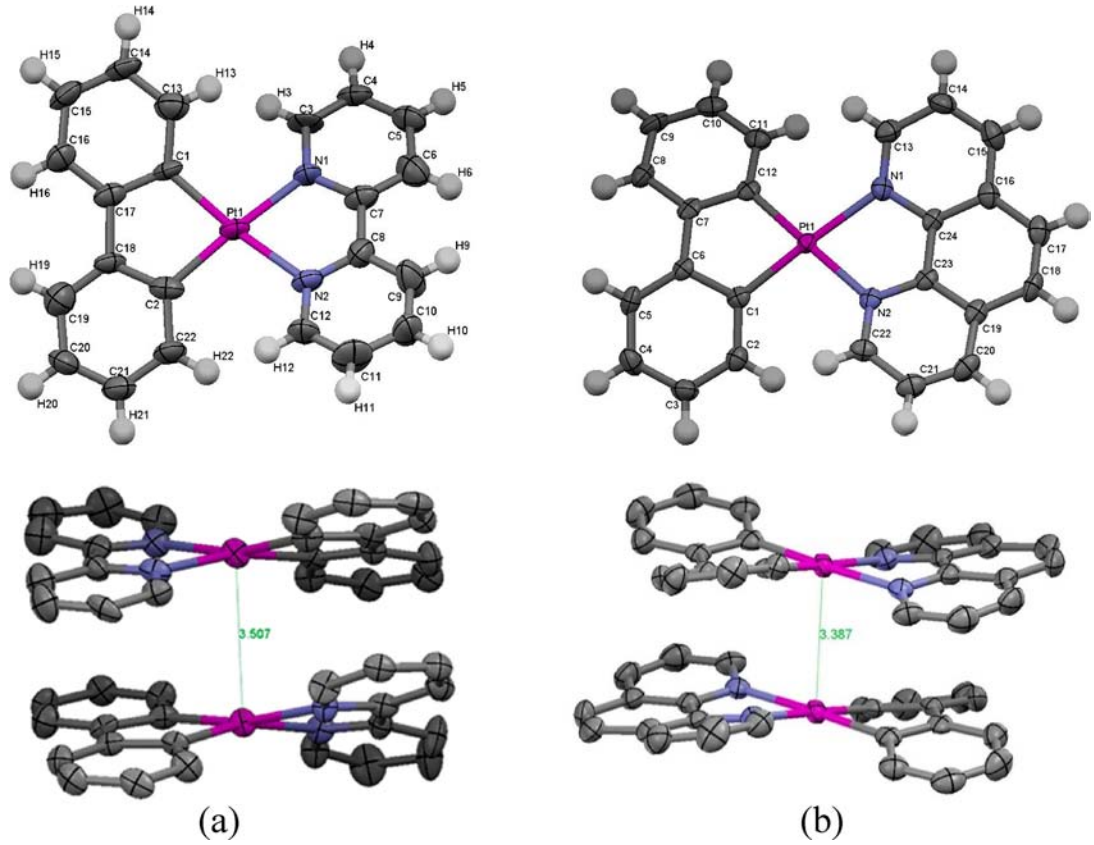

Figure 2. ORTEPs at 50% thermal ellipsoid probability: (a) Pt(bph)(bpy) ; (b) Pt(bph)(phen).

Table 2. Selected Bond Lengths (Å) and Angles (deg) for Pt(bph)(phen) and Pt(bph)(bpy)

Pt(bph)bpy	X-ray	calcd	Pt(bph)phen	X-ray	calcd
		bond length (Å)			
Pt−N1	2.101(8)	2.154	Pt−N1	2.121(2)	2.17
Pt−N2	2.125(8)	2.154	Pt−N2	2.123(2)	2.17
Pt−C1	1.993(9)	2.032	Pt−C1	1.996(3)	2.033
Pt−C2	2.021(10)	2.032	Pt−C2	2.003(3)	2.033
		bond angle (deg)			
C1−Pt−C2	80.2(4)	80.68	C1−Pt−C2	80.55(11)	80.1
N1−Pt−N2	76.6(3)	76.4	N1−Pt−N2	77.68(9)	76.7
C1−Pt−N1	102.5(3)	103.6	C1−Pt−N1	100.30(10)	101.5
C2−Pt−N2	104.1(3)	103.6	C2−Pt−N2	101.38(10)	101.5
		dihedral (deg)			
Pt−C−C−bph*	176.35(5)	179	Pt−C−C-bph*	162.74(7)	160.4
Pt−N−N−bpy *	179.73(6)	176.3	Pt−N−N−phen*	163.15(5)	168.7
C−C−N−N	20.20(3)	30	C−C−N−N	0.33(2)	0.004
		Pt···Pt distance (Å)			
	3.505(6)		Pt···Pt distance (Å)	3.387(4)	

atoms associated in each molecular orbital. Here, localized electron densities are presented in terms of percent orbital distribution (Table 5).

Pt(bph)(bpy). Figure 8 shows frontier molecular orbital pictures of Pt(bph)(bpy) from HOMO-3 to LUMO+3. The orbital distributions are listed in Table 5 while calculated singlet energy state transitions are listed in Table 6. The HOMO is a π orbital derived from the bph ligand whereas the HOMO-5 orbital is a π orbital located on the bpy ligand. The HOMO-1, HOMO-2, HOMO-3, and HOMO-4 orbitals are mainly distributed on the platinum metal center and bph ligand. The LUMO, LUMO+1, LUMO+2, and LUMO+3 are π^* orbitals located on the bpy ligand. The LUMO+4 is a π^* orbital located on bph and the LUMO+5 is located entirely on the platinum metal center.

Three dominant transitions are located at 17 884, 36 493, and 39 818 cm^{-1}. The one located at 17 884 cm^{-1} is a metal−ligand to ligand charge transfer, MLLCT, band associated with a combination of platinum-biphenyl (ML) to bpy ligand charge transfer (LCT) transition, HOMO-1 → LUMO (f = 0.0994). The 36 493 cm^{-1} absorption is a MLLCT transition resulting from an electronic transition from platinum-biphenyl to the bpy ligand, HOMO-10 → LUMO (f = 0.2409). The 39 818 cm^{-1} transition is associated with an LC ($\pi \rightarrow \pi^*$) transition located

dx.doi.org/10.1021/ic301393e | *Inorg. Chem.* 2013, 52, 596−607

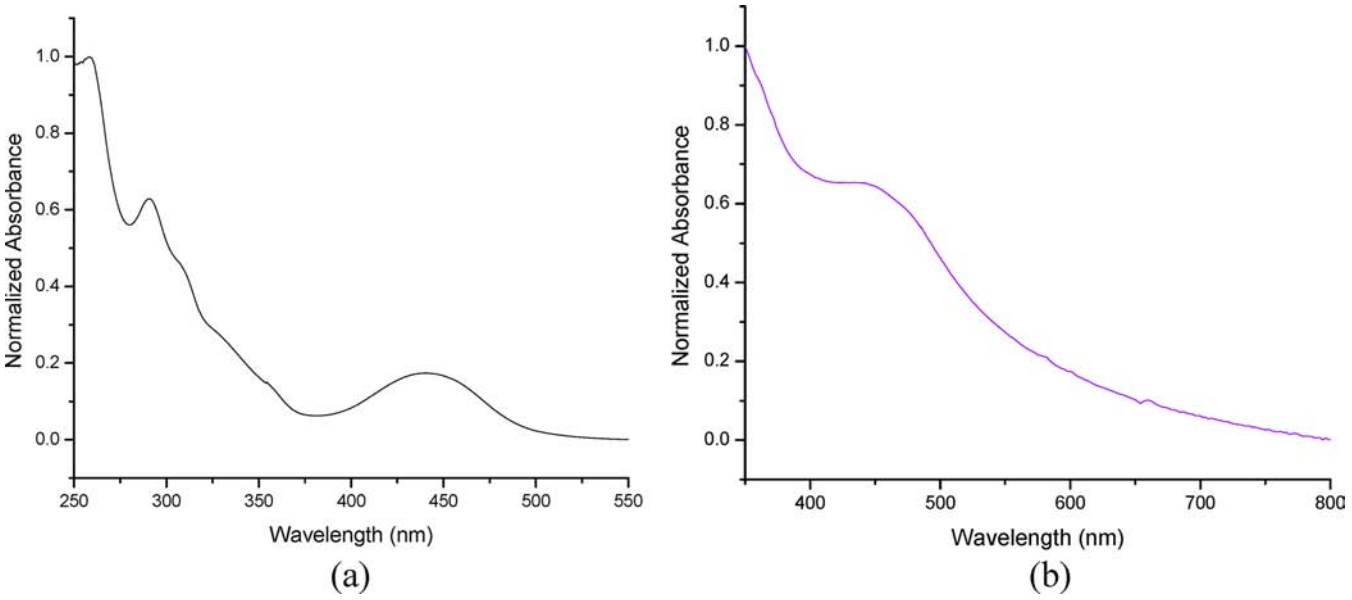

Figure 3. Solution and solid-state UV/visible absorption spectra of Pt(bph)(bpy): (a) in butyronitrile and (b) in KBr.

Table 3. Absorption, Emission, and Electrochemical Data for Pt(bph)(bpy) and Pt(bph)(phen)

	λ_{abs}/nm (ε/$M^{-1}cm^{-1}$) at ambient temperature[a]				
complexes	IL	MLCT	λ_{em}/nm at 77 K[a]	τ/ns at 77 K[a,b]	$E_{1/2red}$/V vs ferrocene/ferrocenium at ambient temp[c]
Pt(bph)(bpy)	226 (2.7×10^4) 258 (2.6×10^4) 289 (1.7×10^4)	440 (5.6×10^3)	578	0.95	−1.410
Pt(bph)(phen)	221 (5.2×10^4) 258 (3.4×10^4) 268 (3.2×10^4)	447 (1.1×10^4)	580	3.61	−1.380

[a]Dried butyronitrile. [b]λ_{ex} = 457 nm [c]0.1 M $TBAPF_6$ in dried acetonitrile

Table 4. Solvent-Dependent Studies Data

			ν_{max} (cm^{-1})	
solvent	dielectric constant (ε)	refractive index (η)	Pt(bph)(bpy)	Pt(bph)(phen)
acetonitrile	37.5	1.3441	23364	23148
propionitrile	27.7	1.3655	23044	22778
butyronitrile	20.7	1.3840	22778	22371
valeronitrile	17.7	1.3970	22523	22173

on bph, HOMO-2 → LUMO+4 (f = 0.4029). There are some other interesting transitions with weak oscillator strengths, e.g., a ligand to ligand charge transfer, LLCT ($\pi \rightarrow \pi^*$), assigned as bph → bpy at 20 035 cm^{-1}, HOMO → LUMO+2 (f = 0.0444), and a metal−ligand to ligand charge transfer, MLLCT, band associated with Pt-bph → bpy at 24 155 cm^{-1}, HOMO-1 → LUMO+1 (f = 0.0477). (See Table S11 of the Supporting Information for HOMO-10 through LUMO+10 data.)

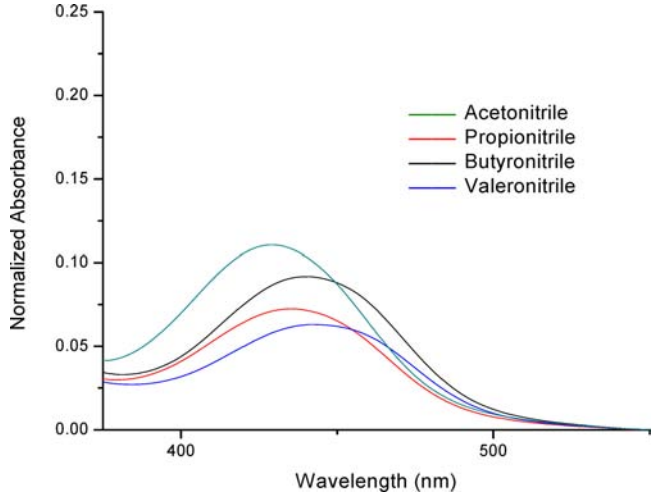

Figure 4. Solvatochromism in MLLCT absorption band for Pt(bph)(bpy).

Pt(bph)(phen). Figure 8 shows pictures of orbitals for Pt(bph)(phen) from HOMO-3 to LUMO+3. In a similar fashion, percent orbital distributions in Pt(bph)(phen) are listed in Table 5 and calculated singlet state energy transitions are shown in Table 7. Theoretical results show that its frontier orbitals are quite similar to those of Pt(bph)(bpy). The HOMO and HOMO-3 are derived from bph π orbitals. The HOMO-1, HOMO-2, and HOMO-4 orbitals are mainly distributed on the platinum metal center and bph ligand. The LUMO to LUMO+3 are π^* orbitals derived from the phen ligand. The principal components of LUMO+4 are the π^* orbitals from bph.

The predominant transitions are located at 18 595, 37 804, and 39 213 cm^{-1} assigned as HOMO-1 → LUMO (f = 0.1365), HOMO-11 → LUMO+1 (f = 0.1156), and HOMO-11 → LUMO (f = 0.1676), respectively. The low-energy transition is a MLLCT band resulting from an electronic transition from platinum-biphenyl to the phen ligand.

UV−Visible Spectra and Solvatochromism. Both Pt(bph)(bpy) and Pt(bph)(phen) complexes gave similar UV−

dx.doi.org/10.1021/ic301393e | Inorg. Chem. 2013, 52, 596−607

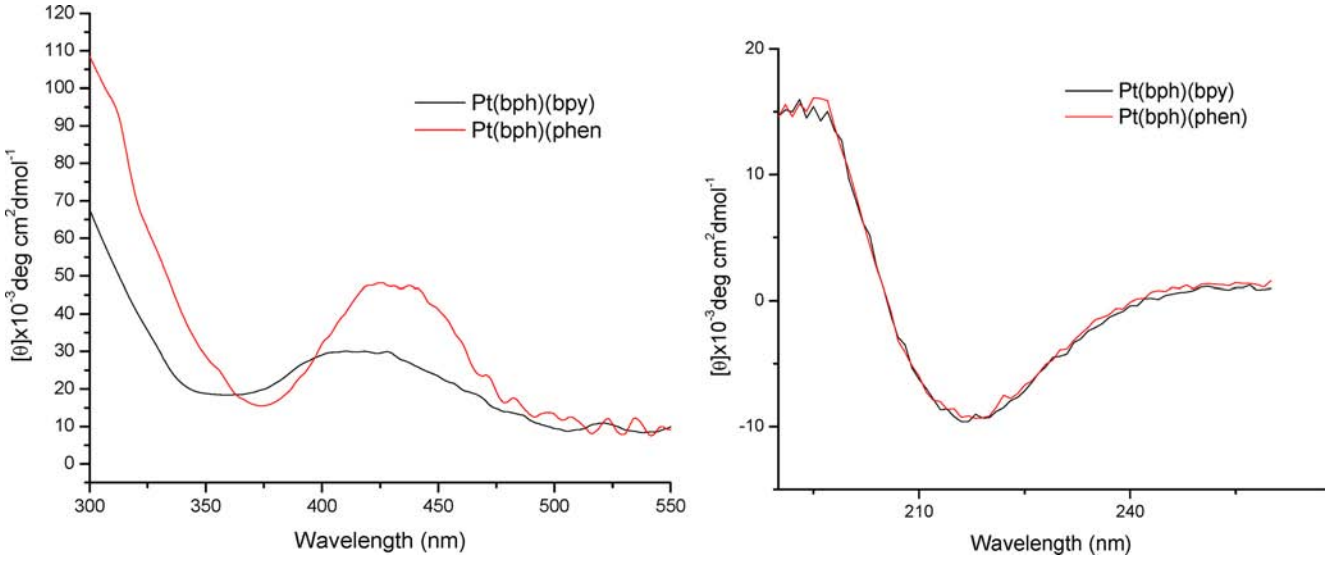

Figure 5. Circular dichroism spectra of Pt(bph)(bpy) and Pt(bph)(phen) in butyronitrile.

vis spectra. The possible assignments of the experimental bands were based on computational assignments of the singlet excited states and related reports of similar types of complexes.[1−3,9] The band at 440 nm was reported before for Pt(bph)(bpy) as MLLCT.[1] Although theoretical assignments resulted in mixing between platinum and biphenyl (i.e. HOMO-2), significant electron density contribution from the platinum supports their strong metallic character. The band at 258 nm is labeled as ligand centered (LC). Figure 9 shows an overlay of the experimental and calculated UV−visible absorption spectra of Pt(bph)(bpy) and Pt(bph)(phen). The comparison of experimental and theoretical absorption maxima are listed in Table 8. Calculations were carried out in the gas phase and as noted from Figure 9, the theoretical maxima are red-shifted compared to the experimental ones. This is often observed when comparisons between gas-phase calculated spectra and experiment ones are made,[44] but allows one to make meaningful transition assignments. The so-called MLLCT band at 440 nm corresponds to an electronic density transition from the Pt/bph to diimine ligand (bpy or phen), not from platinum to bph. Both bpy and phen derivatives have lower unoccupied orbital energies compared to bph and in agreement with Pt(bpy)(en) and Pt(bpy)Cl_2 where the reported MLCT (Pt→bpy) transitions are located at 447 and 394 nm, respectively.[45] The dicarbonyl complex, Pt(bph)$(CO)_2$, also displayed $\pi \rightarrow \pi$ stacking in the solid state, which underwent optical transitions in the visible region located at 580 nm attributed to a $d_{z^2} \rightarrow p_z$ transition.[6]

Complexes lacking a diimine ligand (e.g., Pt(bph)(L) {L = $(C_2H_5)_2S$, py, CH_3CN, en, CO}) have metal-to-ligand transitions from platinum to bph located in the 300−380 nm region.[2,8] In these complexes, the energies of unoccupied orbitals on L are higher compared to bph, therefore allowing electron transfer from the platinum center toward bph. Absorption in the 300 nm region is an over lay of multiple sources of transitions (Tables 6 and 7). In Figure 9, these are represented by vertical blue lines. Based on calculations, MLLCT, LC, and even LLCT have contributions to the bands in this region. In the case of Pt(bph)(phen), there is significant overlap between bph orbitals with Pt(d) atomic orbital in its charge-transfer band (Metal−Ligand-to-Ligand Charge Transfer, MLLCT).

The solvent dependence of the MLLCT band shown in Figure 4 is related to the dipolar nature of the excited state of the complexes. As shown in Figure 10, plots of E_{MLLCT} vs Δf (eq 1), where ε is the dielectric constant of the solvent while η corresponds to solvent refractive index,[46] were linear for both Pt(bph)(bpy) and Pt(bpy)(phen) complexes illustrative of solvatochromism.[46,47]

$$\Delta f = \left[\frac{(\varepsilon - 1)}{(2\varepsilon + 1)} - \frac{(\eta^2 - 1)}{(4\eta^2 + 2)}\right] \quad (1)$$

According to previous studies, the dipole moments of the excited states can be estimated from the slopes of the linear relationship (Figure 10) between E_{MLCT} and Δf as expressed in eq 2, where $\nu_{max}(0)$ is the absorption maximum at the gas phase, h is for Planck's constant, c is the speed of light, and a refers to the effective radius of the solvent shell around the complex, if a is known.[46] Here we estimate a from the longest distance across the Pt(bph)(bpy) and Pt(bph)(phen) molecules from crystal structure data plus van der Waal's radius for the terminal hydrogen atoms[38] to be approximately 4.0×10^{-10} pm for both Pt(bph)(bpy) and Pt(bph)(phen).

$$\nu_{max} = \nu_{max}(0) - 2\mu_e^2 \Delta f / hca^3 \quad (2)$$

The resulting μ_e values determined from the slopes of 27303 $C^2 \cdot s^3 \cdot kg^{-1} \cdot m^{-4}$ for the 2,2′-bipyridine complex and 30219 $C^2 \cdot s^3 \cdot kg^{-1} \cdot m^{-4}$ for the phenanthroline derivative were 12.5 D for Pt(bph)(bpy) and 13.1 D for Pt(bph)(phen). The phenanthroline complex has higher dipole character compared to its 2,2′-bipyridine analogue due to its more extended π-withdrawing character compared to the 2,2′-bipyridine.

Circular Dichroism. Both Pt(bph)(bpy) and Pt(bph)-(phen) gave rise to the same chirality in solution. Since the ligands are not chiral, the chirality must reside in the complexes themselves. The low symmetry suggests the point group associated with the complexes in solution is C_1, which is an optically active point group according to group theory.[39] Multiple CD transitions for the same complex as reported before were observed at charge transfer and d→d transitions.[36]

dx.doi.org/10.1021/ic301393e | Inorg. Chem. 2013, 52, 596−607

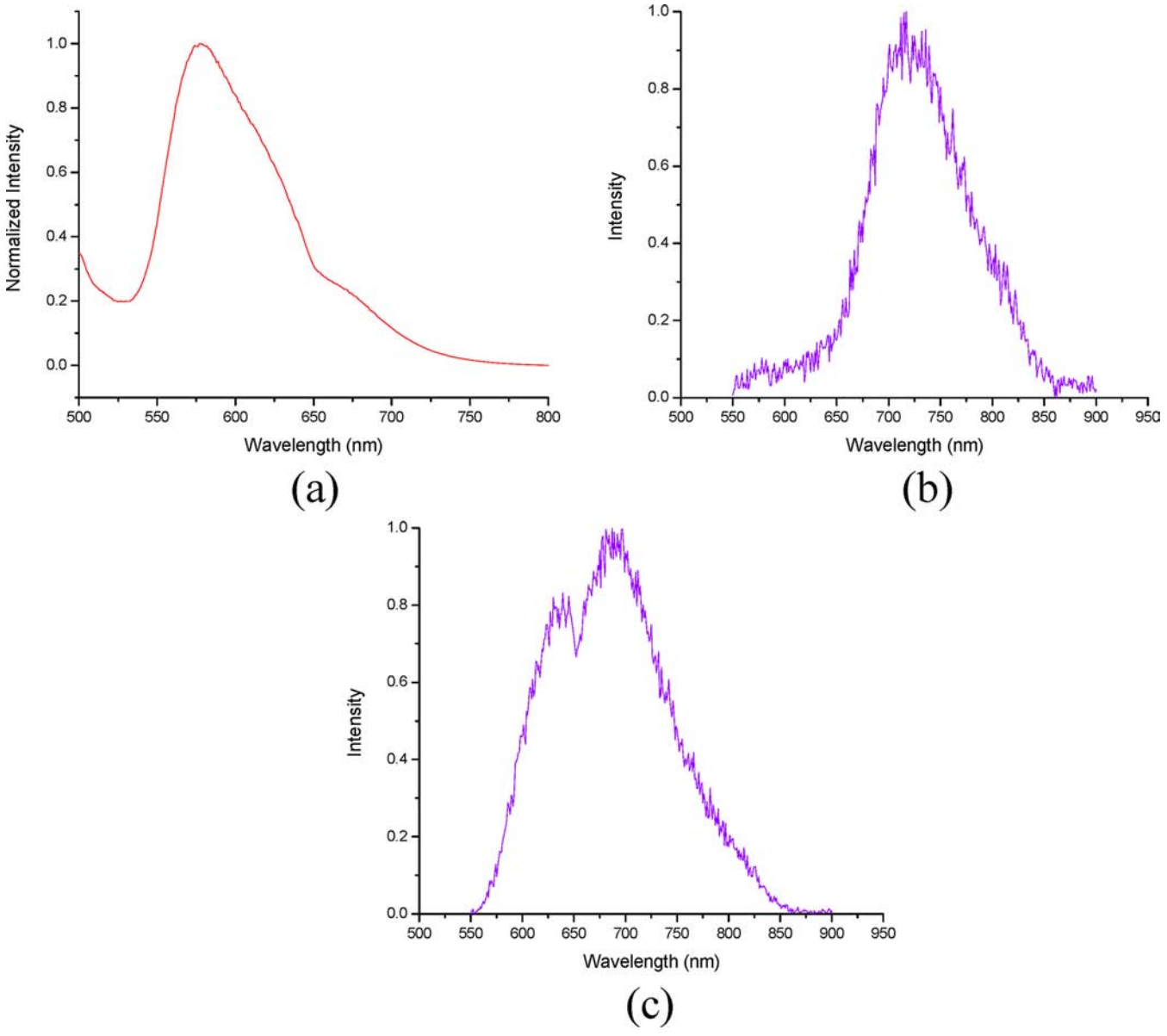

Figure 6. Emission spectra: (a) Pt(bph)(bpy) in butyronitrile (λ_{ex} = 440 nm), (b) Pt(bph)(bpy) in KBr (λ_{ex} = 440 nm), and (c) Pt(bph)(phen) in KBr (λ_{ex} = 447 nm).

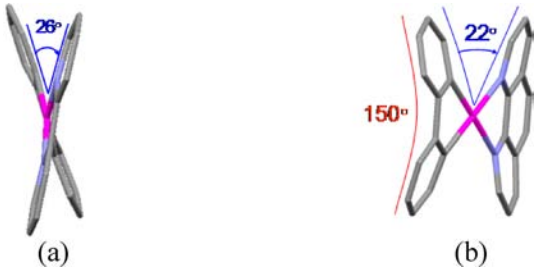

Figure 7. X-ray structures: (a) Pt(bph)(bpy) (X-shaped) and (b) Pt(bph)(phen) (B-shaped).

Similarly here, the CD effect occurs at absorptions related to the complex[36−38] and can be linked to the MLLCT band near 450 nm and d−d transitions buried under the ligand-centered (LC) transitions in the UV region (Figure 9). The metal centered, MC, d→d transitions in the ultraviolet region are predicted from theoretical TDDFT calculations (Tables 6 and

Table 5. Orbital Distributions of Pt(bph)(bpy) and Pt(bph)(phen) from Calculations

	Pt(bph)(bpy)				Pt(bph)(phen)			
molecular orbital	energy level (eV)	Pt (%)	bph (%)	bpy (%)	energy level (eV)	Pt (%)	bph (%)	phen (%)
LUMO+4	−0.27	9	89	2	−0.25	9	89	2
LUMO+3	−0.42	1	0	99	−0.68	1	0	99
LUMO+2	−1.70	1	1	98	−1.35	2	2	96
LUMO+1	−1.84	2	1	97	−2.61	1	0	99
LUMO	−2.70	5	3	92	−2.70	6	3	91
HOMO	−4.71	19	80	1	−4.67	19	80	1
HOMO-1	−5.41	38	51	12	−5.38	38	50	11
HOMO-2	−5.58	28	71	1	−5.54	73	25	2
HOMO-3	−5.59	71	26	2	−5.55	19	80	1
HOMO-4	−6.48	67	26	7	−6.47	68	26	6

dx.doi.org/10.1021/ic301393e | Inorg. Chem. 2013, 52, 596−607

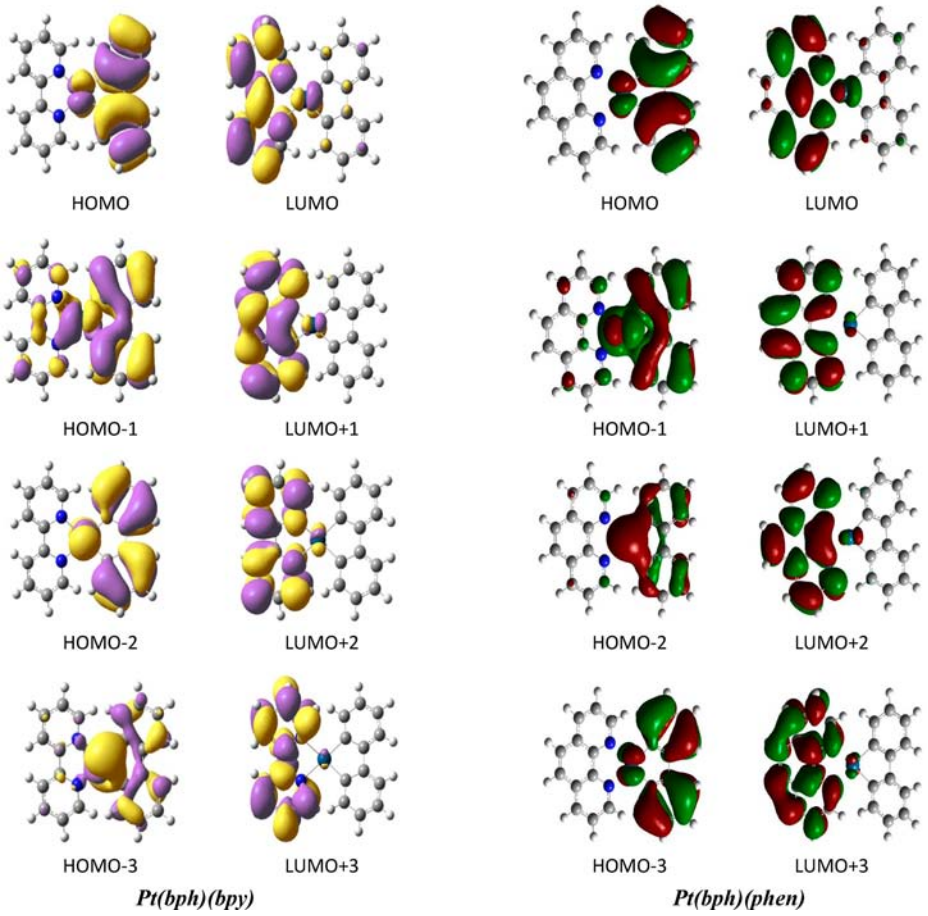

Figure 8. Molecular orbital pictures of Pt(bph)(bpy) and Pt(bph)(phen) where HOMO = highest occupied molecular orbital and LUMO = lowest unoccupied molecular orbital.

Table 6. Calculated Singlet Energy State Transitions for Pt(bph)(bpy)

ν (cm^{-1})	λ (nm)	f	major orbital contributions	nature of transition
17884	559.13	0.0994	HOMO-1 → LUMO (80%)	MLLCT bph, Pt(d) → bpy
20035	499.11	0.0444	HOMO → LUMO+2 (87%)	LLCT bph → bpy
24155	413.99	0.0477	HOMO-1 → LUMO +1 (86%)	MLLCT Pt(d), bph → bpy
30344	329.55	0.0492	HOMO → LUMO+4 (81%)	LC $\pi \rightarrow \pi^*$ (bph)
33298	300.31	0.0459	HOMO-9 → LUMO (44%)	MLLCT bph,Pt(d) → bpy
			HOMO-4 → LUMO +2 (33%)	MLLCT Pt(d),bph → bpy
36493	274.02	0.2409	HOMO-10 → LUMO (54%)	MLLCT bph, Pt(d) → bpy
39818	251.14	0.4029	HOMO-2 → LUMO +4 (41%)	LC $\pi \rightarrow \pi^*$ (bph)
40326	247.98	0.0876	HOMO-3 → LUMO +5 (29%)	MC d → d (Pt)
			HOMO-9 → LUMO +1 (28%)	MLMCT bph,Pt(d) → Pt(d)
			HOMO → LUMO+8 (21%)	LC $\pi \rightarrow \pi^*$ (bph)

Table 7. Calculated Singlet Energy State Transitions for Pt(bph)(phen)

ν (cm^{-1})	λ (nm)	f	major orbital contributions	nature of transition
18595	537	0.1365	HOMO-1 → LUMO (45%)	MLLCT bph,Pt(d) → phen
			HOMO-2 → LUMO (36%)	MLLCT bph,Pt(d) → phen
28723	348	0.0717	HOMO-2 → LUMO+2 (43%)	MLLCT bph,Pt(d) → phen
			HOMO-1 → LUMO+2 (32%)	MLLCT bph,Pt(d) → phen
30690	326	0.0577	HOMO → LUMO+4 (69%)	LC $\pi \rightarrow \pi^*$ (bph)
37804	265	0.1156	HOMO-11 → LUMO +1 (51%)	LC $\pi \rightarrow \pi^*$ (phen)
39213	255	0.1676	HOMO-11→ LUMO (32%)	LC $\pi \rightarrow \pi^*$ (phen)
			HOMO-5 → LUMO+2 (12%)	LC bph → phen
39655	252	0.2562	HOMO-3 → LUMO+4 (44%)	LC $\pi \rightarrow \pi^*$ (bph)
40490	247	0.3147	HOMO-2 → LUMO +8 (17%)	MMLCT Pt(d) → Pt(d),bph
			HOMO-3 → LUMO+4 (17%)	LC $\pi \rightarrow \pi^*$ (bph)
40715	246	0.0224	HOMO-4 → LUMO+3 (82%)	MLCT Pt(d) → phen

7). The strong field dianionic bph ligand is expected to drive up the energy of the d−d state resulting in high energy absorption justifying this assignment.

Emission Studies. The profiles and location of the energy manifolds shown in Figure 11 for Pt(bph)(bpy) and Pt(bph)-

dx.doi.org/10.1021/ic301393e | *Inorg. Chem.* 2013, 52, 596−607

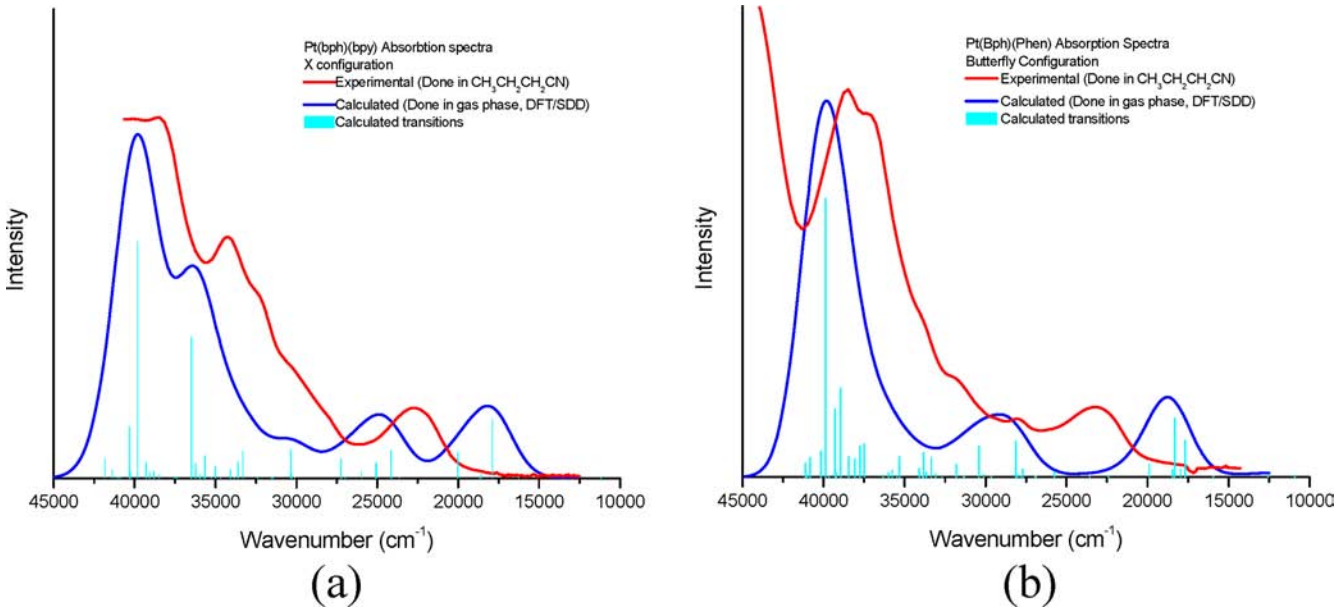

Figure 9. (a) Experimental and calculated electronic absorption spectra of Pt(bph)(bpy). (b) Experimental and calculated electronic absorption spectra of Pt(bph)(phen).

Table 8. Assignments of Absorption Spectra

	experimental[a]		.	
complex	absorption	assignment	transition	assignment
Pt(bph)(bpy)	226		251	LC $\pi \rightarrow \pi^*$ (bph)
	258	MLLCT	274	LC $\pi \rightarrow \pi^*$ (bpy)
	289			
	440	MLLCT	559	MLLCT Pt(d),bph → bpy
Pt(bph)(phen)	221			
	258	LC	252	LC $\pi \rightarrow \pi^*$ (bph)
	268		255	LC $\pi \rightarrow \pi^*$ (phen)
	447	MLLCT	537	MLLCT bph,Pt (d) → phen

[a]Butyronitrile. [b]Gas phase.

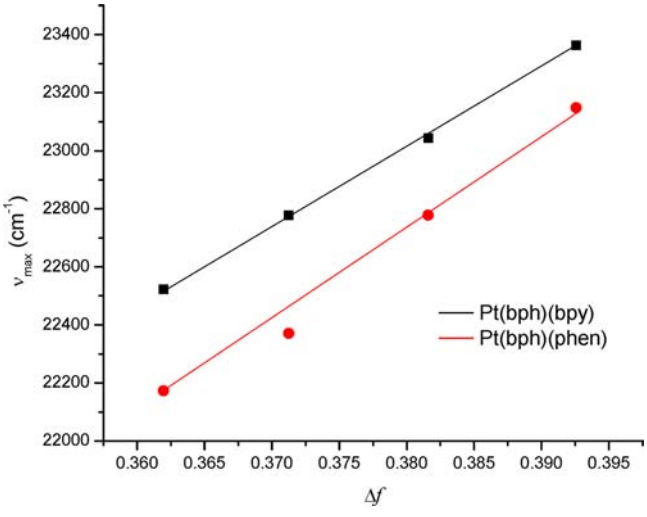

Figure 10. Least-squares regression plots for E_{MLLCT} vs Δf.

(phen) are similar to those associated with ^{3}MLLCT emissions of similar complexes.[48−50] Also shown in Figure 11 are Gaussian bell curve fitting analyses for emission spectra of Pt(bph)(bpy) and Pt(bph)(phen) which can be used to determine vibronic coupling interactions in the glassy state from the peak positions. The spacings between the calculated peaks are 1156 and 1173 cm^{-1} for Pt(bph)(bpy) and 1225 and 1149 cm^{-1} for Pt(bph)(phen) consistent with the assignment of ring-breathing modes as assigned in the past.[49,50]

The short emission lifetimes of 1−3 ns exciting at 457 nm were surprising since emission lifetimes reported for platinum biphenyl complexes were in the microsecond time domain under similar conditions when complexes were excited near 330 nm.[1] We will address this in a future publication.

Solid state emission (Figure 6b,c) was observed in both complexes with its maxima located at 690 nm for Pt(bph)(bpy) and 710 nm for Pt(bph)(phen), respectively. These emission energies are much lower compared to the previously observed emission of $[Pt_2(\mu\text{-}P_2O_5H_2)_4]^{4-}$, which is at 515 nm.[51] A DFT/TDDFT study[52] on ground and excited states of $[Pt_2(\mu\text{-}P_2O_5H_2)_4]^{4-}$ revealed that a decay from its triplet excited state to the ground state could occur from Pt_p,Pt_d to Pt···Pt_σ states in agreement with Krogmann's model.[29]

CONCLUSION

Pt(bph)(bpy) and Pt(bph)(phen) crystallized in the solid state in two configurations designated as X and B related to the orientation of the bph and diimine rings. Due to deviations from square planar geometry, the complexes exhibited chirality in solution. Both complexes underwent MLLCT transitions near 440 nm and emission with nanosecond lifetimes at 77 K. The origin of the emission was ^{3}MLLCT for Pt(bph)(bpy) and Pt(bph)(phen) with structured emission consistent with ring breathing modes. Absorption obtained for the Pt(bph)(bpy) complex in KBr pellets occurred at 440 nm, but emission was found near 700 nm due to $\pi-\pi$ stacking of the complexes resulting from Pt···Pt interactions in the solid state. DFT calculations show the LUMO for both systems is located on the

dx.doi.org/10.1021/ic301393e | Inorg. Chem. 2013, 52, 596−607

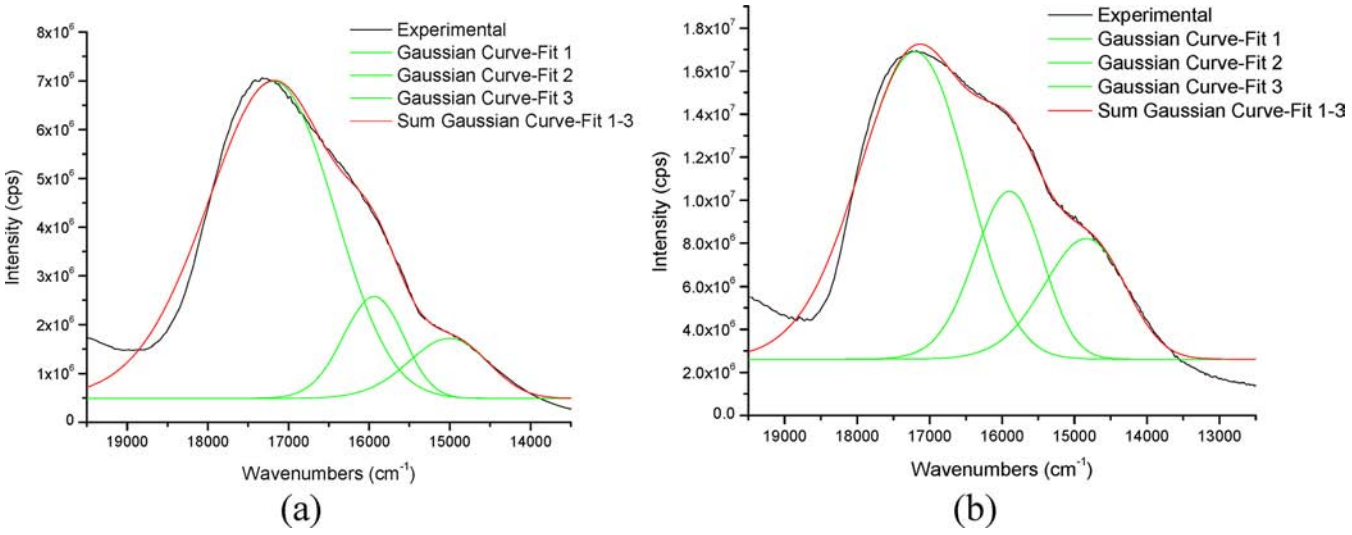

Figure 11. Emission spectra: (a) Pt(bph)(bpy) in butyronitrile (λ_{ex} = 440 nm) and (b) Pt(bph)(phen) (λ_{ex} = 447 nm).

diimine ligand, not on the bph ligand. TDDFT results allow assignment of the low-energy transition to HOMO-1 → LUMO for both complexes. Solvatochromism was observed for both complexes giving rise to excited state dipoles of 12.5 D for Pt(bph)(bpy) and 13.1 D for Pt(bph)(phen).

■ ASSOCIATED CONTENT

Supporting Information

X-ray crystallographic data of [Pt(bph)(bpy)] and [Pt(bph)(phen)] in CIF format and detailed X-ray crystallographic data and orbital distributions of [Pt(bph)(bpy)] and [Pt(bph)(phen)]. This material is available free of charge via the Internet at http://pubs.acs.org.

■ AUTHOR INFORMATION

Corresponding Author

*E-mail: paul.rillema@wichita.edu.

Notes

The authors declare no competing financial interest.

■ ACKNOWLEDGMENTS

We thank the Wichita State University High Performance Computing Center, the Wichita State University Office of Research Administration, the Department of Energy, and NSF-EPSCoR for support.

■ REFERENCES

(1) Maestri, M.; Sandrini, D.; Balzani, V.; von Zelewsky, A.; Cornioley-Deuschel, C.; Jolliet, P. *Helv. Chim. Acta* **1988**, *71*, 1053−1059.

(2) Blanton, C. B.; Murtaza, Z.; Shaver, R. J.; Rillema, D. P. *Inorg. Chem.* **1992**, *31*, 3230−3235.

(3) Blanton, C. B.; Rillema, D. P. *Inorg. Chim. Acta* **1990**, *168*, 145−147.

(4) (a) Yersin, H.; Fischer, T.; Czerwieniec, R.; Monkowius, U. *Int. Appl.* WO 2009112152 A1 20090917, 2009. (b) Yersin, H.; Fischer, T.; Czerwieniec, R.; Monkowius, U. *Ger. Offen.* DE102008013691 A1 20090917, 2009. (c) Yersin, H.; Monlowius, U.; Czerwieniec, R. *Ger. Offen.* DE 102006017485 A1 20071018, 2007.

(5) (a) Plutino, M. R.; Scolaro, L. M.; Albinati, A.; Romeo, R. *J. Am. Chem. Soc.* **2004**, *126*, 6470−6484. (b) Simhai, N.; Iverson, C. N.; Edelbach, B. L.; Jones, W. D. *Organometallics* **2001**, *20*, 2759−2766. (c) Plutino, M. R.; Scolaro, L. M.; Romero, R.; Grassi, A. *Inorg. Chem.* **2000**, *39*, 2712−2720.

(6) Chen, Y.; Woods, C.; Perkovic, M. W.; Rillema, D. P. *J. Chem. Crystallogr.* **1996**, *26*, 527−531.

(7) Zheng, G. Y.; Rillema, D. P. *Inorg. Chem.* **1998**, *37*, 1392−1397.

(8) Chen., Y.; Merkert, J. W.; Murtaza, Z.; Woods, C.; Rillema, D. P. *Inorg. Chim. Acta* **1995**, 41−47.

(9) Cornioley-Deuschel, C.; von Zelewsky, A. *Inorg. Chem.* **1987**, *26*, 3354−3358.

(10) Gilman, H.; Gaj, H. J. *J. Org. Chem.* **1957**, *22*, 447−449.

(11) Gardner, S. A.; Gordon, H. B.; Rausch, M. P. *J. Organomet. Chem.* **1973**, *60*, 179−188.

(12) Kaufmann, G. B.; Cowan, D. O. *Inorg. Synth.* **1960**, *6*, 211−215.

(13) Frisch, M. J.; Trucks, G. W.; Schlegel, H. B.; Scuseria, G. E.; Robb, M. A.; Cheeseman, J. R.; Montgomery, J. A., Jr.; Vreven, T.; Kudin, K. N.; Burant, J. C.; Millam, J. M.; Iyengar, S. S.; Tomasi, J.; Barone, V.; Mennucci, B.; Cossi, M.; Scalmani, G.; Rega, N.; Petersson, G. A.; Nakatsuji, H.; Hada, M.; Ehara, M.; Toyota, K.; Fukuda, R.; Hasegawa, J.; Ishida, M.; Nakajima, T.; Honda, Y.; Kitao, O.; Nakai, H.; Klene, M.; Li, X.; Knox, J. E.; Hratchian, H. P.; Cross, J. B.; Bakken, V.; Adamo, C.; Jaramillo, J.; Gomperts, R.; Stratmann, R. E.; Yazyev, O.; Austin, A. J.; Cammi, R.; Pomelli, C.; Ochterski, J. W.; Ayala, P. Y.; Morokuma, K.; Voth, G. A.; Salvador, P.; Dannenberg, J. J.; Zakrzewski, V. G.; Dapprich, S.; Daniels, A. D.; Strain, M. C.; Farkas, O.; Malick, D. K.; Rabuck, A. D.; Raghavachari, K.; Foresman, J. B.; Ortiz, J. V.; Cui, Q.; Baboul, A. G.; Clifford, S.; Cioslowski, J.; Stefanov, B. B.; Liu, G.; Liashenko, A.; Piskorz, P.; Komaromi, I.; Martin, R. L.; Fox, D. J.; Keith, T.; Al-Laham, M. A.; Peng, C. Y.; Nanayakkara, A.; Challacombe, M.; Gill, P. M. W.; Johnson, B.; Chen, W.; Wong, C. Gonzalez, M. W.; Pople, J. A. *Gaussian 03*, Revision B.04, Gaussian, Inc.: Wallingford CT, 2004.

(14) Becke, A. D. *J. Chem. Phys.* **1993**, *98*, 5648−5653.

(15) Lee, C.; Yang, W.; Parr, R. G. *Phys. Rev. B* **1988**, *37*, 785−789.

(16) Vosko, S. H.; Wilk, L.; Nusair, M. *Can. J. Phys.* **1980**, *58*, 1200−1211.

(17) (a) Stratmann, R. E.; Scuseria, G. E.; Frisch, M. *J. Chem. Phys.* **1998**, *109*, 8218−8225. (b) Bauernschmitt, R.; Ahlrichs, R. *Chem. Phys. Lett.* **1996**, *256*, 454−464. (c) Casida, M. E.; Jamorski, C.; Casida, K. C.; Salahub, D. R. *J. Chem. Phys.* **1998**, *108*, 4439−4450.

(18) (a) Cossi, M.; Barone, V. *J. Chem. Phys.* **2001**, *115*, 4708−4718. (b) Barone, V.; Cossi, M. *J. Phys. Chem. A* **1998**, *102*, 1995−2001. (c) Cossi, M.; Rega, N.; Scalmani, G.; Barone, V. *J. Comput. Chem.* **2003**, *24*, 669−681.

(19) Stoyanov, S. R.; Villegas, J. M.; Rillema, D. P. *Inorg. Chem.* **2002**, *41*, 2941−2945.

(20) O'Boyle, N. M.; Tenderholt, A. L.; Langner, K. M. *J. Comput. Chem.* **2008**, *29*, 839−845.
(21) Rudolph, M.; Autschbach, J. *J. Phys. Chem. A* **2011**, *115*, 2635−2649.
(22) (a) *Bruker APEX2 User Manual*, 2006; Brucker AXS Inc.: Madison, WI, USA. (b) Schdrick, G. M. *SHELXS97 and SHELXL97* 1997, University of Gottingen, Germany. (c) Johnson, C. K. *ORTEP − A FORTRAN Thermal Ellipsoid Plot Program*; Technical Report ORNL-5138; Oak Ridge, TN, 1976.
(23) Mdleleni, M. M.; Bridgewater, J. S.; Watts, R. J.; Ford, P. C. *Inorg. Chem.* **1995**, *34*, 2334−2342.
(24) Chassot, L.; Muller, E.; von Zelewsky, A. *Inorg. Chem.* **1984**, *23*, 4249−4253.
(25) Dong, V.; Keller, H. J.; Moroni, W.; Nothe, D. *Acta Crystallogr., Sect. B: Struct. Crystallogr. Cryst. Chem.* **1977**, *B33*, 2428−2431.
(26) Endres, H.; Keller, H. J.; Moroni, W.; Nothe, D.; Dong, V. *Acta Crystallogr., Sect. B: Struct. Crystallogr. Cryst. Chem.* **1978**, *B34*, 1823−1827.
(27) Hazell, A.; Mukhopadhyay, A. *Acta Crystallogr., Sect. B: Struct. Crystallogr. Cryst. Chem.* **1980**, *B36*, 1647−1649.
(28) Michelin, R. A.; Bertani, R.; Mozzon, M.; Bombieri, G.; Benetollo, F.; de Fatima, M.; da Silva, C. G.; Pombiero, A. J. L. *Organometallics* **1993**, *12*, 2372−2376.
(29) Krogmann, K. *Angew. Chem., Int. Ed. Engl.* **1969**, *8*, 35−42.
(30) Osborn, R. S.; Rogers, D. *J. Chem. Soc., Dalton Trans.* **1974**, 1002−1004.
(31) (a) Thomas, T. W.; Underhill, A. E. *Chem. Soc. Rev.* **1972**, *1*, 99−120. (b) Iball, J.; Macdougall, M.; Scrimgeous, S. *Acta Crystallogr., Sect. B: Struct. Crystallogr. Cryst. Chem.* **1975**, *31*, 1672−1674.
(32) Che, C.-M.; He, L.-Y.; Poon, C.-K.; Mack, T. C. W. *Inorg. Chem.* **1989**, *28*, 3081−3083.
(33) Krogmann, K. Z. *Z. Naturforsch.* **1968**, *28*, 1012.
(34) (a) Buss, C. E.; Anderson, C. E.; Pomije, M. K.; Lutz, C. M.; Britton, D.; Mann, K. R. *J. Am. Chem. Soc.* **1998**, *120*, 7783−7790. (b) Buss, C. E.; Mann, K. R. *J. Am. Chem. Soc.* **2002**, *124*, 1031−1039. (c) Hazell, A.; Mukhopadhyay, A. *Acta Crystallogr., Sect. B: Struct. Crystallogr. Cryst. Chem.* **1980**, *B36*, 1647−1649.
(35) Rudolph, M.; Ziegler, T.; Autschbach, J. *J. Chem. Phys. A* **2011**, *115*, 2635−2649.
(36) Autschbach, J.; Jorge, F. E.; Ziegler, T. *Inorg. Chem.* **2003**, *42*, 2867−2877.
(37) Hazell, A.; Simonsen, O.; Wernberg, O. *Acta Crystallogr., Sect. C: Cryst. Struct. Commun.* **1986**, *42*, 1707−1711.
(38) Stephens, P. J.; Harada, N. *Chirality* **2010**, *22*, 229−233.
(39) Huheey, J. E.; Keitner, E. A.; Keitner, R. L. *Inorganic Chemistry*; 4th ed.; HarperCollins: New York, NY, 1992; p 64.
(40) (a) Martin, J. M. L.; Sundermann, A. *J. Chem. Phys.* **2001**, *114*, 3408−3421. (b) Kim, K.; Jordan, K. D. *J. Phys. Chem.* **1994**, *98*, 10089−10094. (c) Steele, R. P.; DiStasio, R. A.; Shao, Y.; Kong, J.; Head-Gordon, M. *J. Chem. Phys.* **2006**, *125*, 74108.
(41) Bittner, M.; Koppel, H. *J. Phys. Chem. A* **2004**, *108*, 11116−11126.
(42) Yang, Y.; Weaver, M. N.; Merz, K. M. *J. Phys. Chem. A* **2009**, *113*, 9843−9851.
(43) (a) Wachter, A. J. H. *J. Chem. Phys.* **1970**, *52*, 1033−1036. (b) Rappe, A. K.; Smedley, T.; Goddard, W. A., III *J. Phys. Chem.* **1981**, *85*, 2607−2611. (c) Stevens, W.; Basch, H.; Krauss, J. *J. Chem. Phys.* **1984**, *81*, 6026−6034. (d) Check, C. E.; Faust, T. O.; Bailey, J. M.; Wright, B. J.; Gilbert, T. M.; Sunderlin, L. S. *J. Phys. Chem. A* **2001**, *105*, 8111−8116.
(44) (a) Andrae, D.; Hauessermann, U.; Dolg, M.; Stoll, H.; Preuss, H. *Theor. Chim. Acta* **1990**, *77*, 123−141. (b) Gao, H.; Wei, X.; Liu, X.; Yan, T. *J. Phys. Chem. B* **2010**, *114*, 4056−4062. (c) Cruz, A. J.; Kirgan, R.; Siam, K.; Heiland, P.; Rillema, D. P. *Inorg. Chim. Acta* **2010**, *363*, 2496−2505.
(45) Houlding, V. H.; Miskowsky, V. M. *Coord. Chem. Rev.* **1991**, *111*, 145−152.
(46) Fukuzumi, S.; Tokuda, Y.; Fujita, M. *J. Phys. Chem.* **1992**, *96*, 8413−8416.
(47) Manuta, D. M.; Lees, A. J. *Inorg. Chem.* **1986**, *25*, 3212−3218.
(48) Blanton, C. B.; Murtaza, Z.; Shaver, R. J.; Rillema, D. P. *Inorg. Chem.* **1992**, *31*, 3230−3235.
(49) Chen, Y. H.; Merkert, J. W.; Murtaza, Z.; Woods, C.; Rillema, D. P. *Inorg. Chim. Acta* **1995**, *240*, 41−47.
(50) Stoyanov, S. R.; Villegas, J. M.; Rillema, D. P. *J. Phys. Chem. B* **2004**, *108*, 12175−12180.
(51) Kumaresan, D.; Lebkowsky, K.; Schmehl, R. H. *J. Photochem. Photobiol., A* **2009**, *207*, 86−93.
(52) (a) Roundhill, D. M.; Sperline, R. P.; Beaulieu, W. B. *J. Chem. Soc., Chem. Commun.* **1977**, *1*, 62−63. (b) Che, C.-M.; Butler, L. G.; Gray, H. B. *J. Am. Chem. Soc.* **1981**, *103*, 7769−7797. (c) Rice, S. F.; Gray, H. B. *J. Am. Chem. Soc.* **1983**, *105*, 4571−4575. (d) Fordyce, W. A.; Brummer, J. G.; Crosby, G. A. *J. Am. Chem. Soc.* **1981**, *10*, 7061−7064.